CILAMCE 2017
Florianópolis - Santa Catarina - Brazil

PERFORMANCE ANALYSYS OF THE DIRECT INTEGRATION TECHNIQUE FOR SOLVING EIGENVALUE PROBLEMS WITH NON-REGULAR DOMAINS

Carlos Friedrich Loeffler

Hércules de Melo Barcelos

carlosloeffler@bol.com.br

engercules@gmail.com

Programa de Pós Graduação em Engenharia Mecânica, PPGEM/UFES

Av. Fernando Ferrari 514 – Bairro Goiabeiras, Vitória, ES – CEP 29075-910

Abstract. *The aim of this work is evaluate the performance of the Direct Interpolation Boundary Element Formulation (DIBEM) in the solution of Helmholtz problems that present non regular geometric shapes. Using the radial basis functions, the DIBEM approximates the non-self adjoint kernel of the domain integral equations, which appear in many partial differential equations of the mathematical, physics and engineering. Modeling the Helmholtz Equation, the DIBEM approximates the inertia term by a sequence of radial basis functions. The technique has been successfully used previously in Poisson and Helmholtz problems, considering regular geometries and taking analytical solutions as reference for performance evaluation. In this paper, the effects of slenderness of the domain and the introduction of grooves in the boundary are evaluated. Reference solutions are generated through simulation with the Finite Element Method using a fine mesh.*

Keywords: *Boundary elements, Helmholtz's equation, Eigenvalues problems, Irregular geometric conformation*

1 INTRODUCTION

Nowadays, the RBF's are intensively used in meshless formulations that belong the context of the Finite Element Method. However, the Dual Reciprocity Boundary Element Method (DRBEM) (Nardini e Brebbia, 1982; Partridge, 1992) was the pioneer discrete technique concerning the use of Radial Base Functions (RBF) (Buhmann, 2003; Shaback, 2007) as auxiliary tool in mathematical modeling. Using the DRBEM technique, radial basis functions are used to interpolate the dependent variable present in the kernel of domain integrals as occurs in problems that have non-self-adjunct operators in their governing equations. This is the case of dynamic problems, due to the inertia effects, but there are many other important situations such as the diffusive-advective problems, for example. Furthermore, RBFs avoids the use of complicated fundamental solutions allowing the use of simpler homogeneous and stationary fundamental solution. However, there are many restrictions associated to the performance of radial functions in DRBEM. Such functions present satisfactory precision just in sets of dates reasonable size (Chen et al., 1999); some tests showed that certain RBFs fail to certain applications and are successful in others, especially when the same function is tested in problems with two or three dimensions (Bueno and Partridge, 2011; Bueno and Partridge, 2013). Others researchers indicate lack of convergence when RBF's are used in set with iterative (Cheng, Young and Tsai, 2000).

Recently a new formulation called the Direct Interpolation Boundary Element Method (DIBEM) has been developed. It uses the RBFs in a more similar way to the interpolation procedure than DRBEM, since it approximates directly the complete kernel of the domain integrals by a set of known functions with coefficients to determinate. It also transforms the domain integrals into boundary integral by using a primitive radial basis function.

The DIBEM was successfully applied to Poisson and Helmholtz problems, using the classical RBFs (Loeffler et al., 2015, Loeffler et al, 2016) as classical simple radial, thin plate radial and cubic radial. The modern and well known Wendland (Wendland, 1995) and Wu (Wu, 1995) functions also were evaluated, using complete and compact supports (CRBFs), but initial conclusions indicate that many of these functions, widely used in FEM meshless applications, did not perform acceptable even using full support, especially those of higher order. In fact, the CRBFs were used not for the purpose of limiting their radius of action, but because they possess important mathematical properties: they are definite positives and form matrices with dominant diagonals, which would result in greater precision in the solution of the final system of discrete equations. The results showed that only one Wendland function performed similarly to classical radial functions.

Regarding problems with non smooth boundaries, that is, boundaries that present cuts or insertions the DIBEM formulation do not still suitably analyzed. Thus, the objective of this paper is to simulate problems with irregular domains, since in these cases appear greater numerical difficulties, allowing a better evaluation of the robustness of the DIBEM. However, based to the performance previously evaluated, only the thin plate function and the third power Wendland function were here used on the numerical simulations.

A particular and interesting scalar problem that allows an accurate performance evaluation of the DIBEM capability is the eigenvalue problem. Solving the eigenvalue problem it is possible to compare suitably the calculated numerical values of frequencies with results achieved by the available analytical formulas or then, obtained by a robust numerical method employing a very refined mesh.

2 INTEGRAL FORMULATION

Consider the Helmholtz equation in its inverse integral formulation (Brebbia and Walker, 1980), given by:

$$c(\xi)u(\xi)+\int_{\Gamma}u(X)q^*(\xi;X)d\Gamma-\int_{\Gamma}q(X)u^*(\xi;X)d\Gamma=\frac{1}{k^2}\omega^2\int_{\Omega}u(X)u^*(\xi;X)d\Omega \tag{1}$$

In Eq. (1), u(X) is the scalar potential and q(X) is its normal derivative; u*(ξ, X) is the fundamental solution and q*(ξ, X) is its normal derivative. The scalar ω is the imposed frequency of excitation, k represents the stiffness term and the coefficient c(ξ) depends on the positioning of the point ξ with respect to the physical domain Ω (X).

Using the DIBEM, the fundamental solution also comprises the kernel of integral to be interpolated and so that the source point ξ can have the same position as the field X points, it is necessary to carry out a regularization procedure, similar to Hadamard's (Braga, 2006). Therefore, it is done:

$$\begin{aligned}&c(\xi)u(\xi)+\int_{\Gamma}u(X)q^*(\xi;X)d\Gamma-\int_{\Gamma}q(X)u^*(\xi;X)d\Gamma=\\&\frac{1}{k^2}w^2\{\int_{\Omega}[u(X)u^*(\xi;X)]d\Omega-\int_{\Omega}[u(\xi)u^*(\xi;X)]d\Omega\}+\frac{1}{k^2}\omega^2\int_{\Omega}[u(\xi)u^*(\xi;X)]d\Omega\end{aligned} \tag{2}$$

Now the two first integrals on the right hand side of Eq. (2) are approximated as follows:

$$\frac{1}{k^2}\omega^2\{\int_{\Omega}[u(X)u^*(\xi;X)]d\Omega-\int_{\Omega}[u(\xi)u^*(\xi;X)]d\Omega\}\approx\frac{1}{k^2}\omega^2\{\int_{\Omega}{}^{\xi}\alpha^jF^j(X^j;X)d\Omega\} \tag{3}$$

In Eq. (3) F^j $(X^j;X)$ is the RBF chosen to the interpolation. For each source point ξ, the interpolation of the DIBEM corresponds to a scan of all the base points X^j relatively to the points X of the domain, weighted by the coefficients ${}^{\xi}\alpha^j$. A primitive function ψ^j is used to transform the domain integral into a contour integral, that is:

$$\begin{aligned}&\int_{\Omega}{}^{\xi}\alpha^jF^j(X^j;X)d\Omega=\int_{\Omega}({}^{\xi}\alpha^j\psi^j_{,ii}(X^j;X))d\Omega\ =\\&{}^{\xi}\alpha^j\int_{\Gamma}\psi^j_{,i}(X^j;X)n_i(X)d\Gamma={}^{\xi}\alpha^j\int_{\Gamma}\eta^j(X^j;X)d\Gamma\end{aligned} \tag{4}$$

The mathematical transformation presented in Eq. (4) was tested and gave quite satisfactory results in preliminary applications related to calculations of volumes and image values of two-dimensional functions (Loeffler et al., 2016). However, there is loss of precision and this transformation is certainly responsible for the numerical problems presented by high order CRBFs, even with full support, in conjunction with matrix conditioning aspects.

Turning to Eq. (2), the latter term on the right-hand side of this can be transformed into a boundary integral, using the Galerkin Tensor G* concept (Brebbia et al., 1984):

$$\int_\Omega [\mathrm{u}(\xi)\mathrm{u}^*(\xi;\mathrm{X})]d\Omega = \mathrm{u}(\xi)\int_\Omega [G^*_{,ii}(\xi;\mathrm{X})]d\Omega = \mathrm{u}(\xi)\int_\Gamma [G^*_{,i}(\xi;\mathrm{X})\mathrm{n}_i(\mathrm{X})]d\Gamma \qquad (5)$$

Substituting Eq. (4) and (5) into Eq. (1) and using the typical MEC discretization procedures, where “n” source points are composed by the sum of internal values and boundary nodal points, the matrix system given by Eq. (6) is obtained. Details can be found in Loeffler et al., 2006.

$$\begin{pmatrix} \mathrm{H}_{11}\ \dots\ \mathrm{H}_{1n} \\ \dots \\ \mathrm{H}_{n1}\dots\dots\mathrm{H}_{nn} \end{pmatrix}\begin{pmatrix} \mathbf{u}_1 \\ \\ \mathbf{u}_n \end{pmatrix} - \begin{pmatrix} \mathrm{G}_{11}\ \dots\ \mathrm{G}_{1n} \\ \dots \\ \mathrm{G}_{n1}\dots\dots\mathrm{G}_{nn} \end{pmatrix}\begin{pmatrix} \mathbf{q}_1 \\ \\ \mathbf{q}_n \end{pmatrix} = \frac{\omega^2}{k^2}\begin{pmatrix} {}^1\alpha^1\dots{}^1\alpha^m \\ \dots\dots\dots\dots \\ {}^n\alpha^1\dots{}^n\alpha^m \end{pmatrix}\begin{pmatrix} \mathrm{N}_1 \\ \dots \\ \mathrm{N}_m \end{pmatrix} - \frac{\omega^2}{k^2}\begin{pmatrix} \mathrm{Z}_1 \\ \dots \\ \mathrm{Z}_n \end{pmatrix} \qquad (6)$$

Where:

$$\begin{pmatrix} Z_1 \\ Z_2 \\ \dots \\ Z_n \end{pmatrix} = \begin{pmatrix} [\int_1 {}^1P^1 d\Gamma_1 + \int_1 {}^1P^2 d\Gamma_2 + \dots + \int_1 {}^1P^n d\Gamma_n] & 0 & \dots\dots & 0 \\ 0 & [\int_1 {}^2P^1 d\Gamma_1 + \int_1 {}^2P^2 d\Gamma_2 + \dots + \int_1 {}^2P^n d\Gamma_n] & \dots\dots & 0 \\ \dots\dots\dots & & & \\ 0 & 0 & \dots & [\int_1 {}^nP^1 d\Gamma_1 + \int_1 {}^nP^2 d\Gamma_2 + \dots + \int_1 {}^nP^n d\Gamma_n] \end{pmatrix}\begin{pmatrix} \mathbf{u}_1 \\ \mathbf{u}_2 \\ \dots \\ \mathbf{u}_n \end{pmatrix} \qquad (7)$$

The coefficients ${}^\xi\alpha^i$ are the unknowns. These can be obtained through the solution of the following system of algebraic equations, which contains a diagonal matrix Λ, composed of the values of the fundamental solution:

$$[{}^\xi\boldsymbol{\alpha}] = [\mathbf{F}]^{-1}[{}^\xi\boldsymbol{\Lambda}][\mathbf{F}]\boldsymbol{\alpha} = [\mathbf{F}]^{-1}[{}^\xi\boldsymbol{\Lambda}][\mathbf{u}] \qquad (8)$$

For each source point it is possible to change the order of the matrix product given by the right hand side of Eq. (7), so that the potential in nodal points **u** appears explicitly, that is:

Proceedings of the XXXVIII Iberian Latin-American Congress on Computational Methods in Engineering
P.O. Faria, R.H. Lopez, L.F.F. Miguel, W.J.S. Gomes, M. Noronha (Editores), ABMEC, Florianópolis, SC, Brazil, November 5-8, 2017.

$$A_\xi = \begin{pmatrix} N_1 & N_2 \dots & N_m \end{pmatrix} \begin{pmatrix} {}^\xi\alpha_1 \\ \dots \\ {}^\xi\alpha_m \end{pmatrix} \tag{9}$$

Then, the components of the vector A_ξ are given by:

$$\begin{pmatrix} A_1 \\ A_2 \\ \dots \\ A_n \end{pmatrix} = \begin{pmatrix} [-S_2\,{}^1\Lambda^2 - S_3\,{}^1\Lambda^3 \dots - S_n\,{}^1\Lambda^n] & S_2\,{}^1\Lambda^2 & \dots\dots & S_n\,{}^1\Lambda^n \\ S_1\,{}^2\Lambda^1 & [-S_1\,{}^2\Lambda^1 - S_3\,{}^2\Lambda^3 \dots - S_n\,{}^2\Lambda^n] & \dots\dots & S_n\,{}^2\Lambda^n \\ \dots\dots\dots & & & \\ S_1\,{}^n\Lambda^1 & S_2\,{}^n\Lambda^2 & \dots & [-S_1\,{}^n\Lambda^1 - S_2\,{}^n\Lambda^3 \dots - S_{n-1}\,{}^n\Lambda^{n-1}] \end{pmatrix} \begin{pmatrix} \mathbf{u}_1 \\ \mathbf{u}_2 \\ \dots \\ \mathbf{u}_n \end{pmatrix} \tag{10}$$

The final matrix system can be written as:

$$\begin{pmatrix} H_{11} \,..\, H_{1n} \\ \dots. \\ H_{n1} \dots H_{nn} \end{pmatrix} \begin{pmatrix} \mathbf{u}_1 \\ \\ \mathbf{u}_n \end{pmatrix} - \begin{pmatrix} G_{11} \,..\, G_{1n} \\ \dots. \\ G_{n1} \dots G_{nn} \end{pmatrix} \begin{pmatrix} \mathbf{q}_1 \\ \\ \mathbf{q}_n \end{pmatrix} = \frac{\omega^2}{k^2} \begin{pmatrix} (A_1 - Z_1) \\ \dots.. \\ (A_n - Z_n) \end{pmatrix} = \frac{\omega^2}{k^2} \begin{pmatrix} M_{11} \,..\, M_{1n} \\ \dots. \\ M_{n1} \dots M_{nn} \end{pmatrix} \begin{pmatrix} \mathbf{u}_1 \\ \\ \mathbf{u}_n \end{pmatrix} \tag{11}$$

3 BEM EIGENVALUE MODEL

The BEM model is mixed model being composed by potential values and normal potential derivatives as well. Thus, Eq. (11) must be manipulated to represent suitably the problem of eigenvalue, which corresponds to the problem of free vibration. Using submatrices (Loeffler & Mansur, 1986) to highlight prescribed values of u and q, one has:

$$\begin{pmatrix} H_{u\bar{u}} & H_{u\bar{q}} \\ H_{q\bar{u}} & H_{q\bar{q}} \end{pmatrix} \begin{pmatrix} \bar{u} \\ u \end{pmatrix} - \begin{pmatrix} G_{u\bar{u}} & G_{u\bar{q}} \\ G_{q\bar{u}} & G_{q\bar{q}} \end{pmatrix} \begin{pmatrix} q \\ \bar{q} \end{pmatrix} = \frac{\omega^2}{k^2} \begin{pmatrix} M_{u\bar{u}} & M_{u\bar{q}} \\ M_{q\bar{u}} & M_{q\bar{q}} \end{pmatrix} \begin{pmatrix} \bar{u} \\ u \end{pmatrix} \tag{12}$$

Considering that for this type of problem the prescribed nodal values of u (X) and q (X) are null and eliminating the derivative of potential q, the following equations is obtained:

$$[\overline{H}]\{u\} = \frac{\omega^2}{k^2}[\overline{M}]\{u\} \tag{13}$$

Proceedings of the XXXVIII Iberian Latin-American Congress on Computational Methods in Engineering
P.O. Faria, R.H. Lopez, L.F.F. Miguel, W.J.S. Gomes, M. Noronha (Editores), ABMEC, Florianópolis, SC, Brazil, November 5-8, 2017.

Where the following auxiliary matrices are used:

$$[\overline{H}] = [H_{qq}] - [G_{qu}][G_{uu}]^{-1}[H_{uq}]$$
$$[\overline{M}] = [M_{qq}] - [G_{qu}][G_{uu}]^{-1}[M_{uq}] \quad (14)$$

4 RADIAL BASIS FUNCTIONS

Table 1 shows the two radial basis functions used in this work. These were chosen for the good performance shown in previous works, already cited. In this table, δ means the value of the support and it is taken as full in all simulations. The variable "r" means the distance between the base points and the field.

Table 1. Radial basis functions

Type of radial basis function	Mathematical formula	Associated primitives
Thin plate	$F^j(r) = \left(\frac{r}{\delta}\right)^2 ln(r/\delta)$	$\psi_{,i} = \frac{1}{\delta^2}\left[-\frac{r^2}{16} + \frac{r^2 \ln r}{4}\right] r_i$
Wendland	$F^j(r) = \left[1 - \frac{r}{\delta}\right]_+^3$	$\psi_{,i} = \left[\frac{1}{2} - \left(\frac{r}{\delta}\right) + \frac{3}{4}\left(\frac{r}{\delta}\right)^2 - \frac{1}{5}\left(\frac{r}{\delta}\right)^3\right] r_i$

5 EXAMPLES

Three examples are solved hereinafter comprising several tests on each of them, using two or three distinct meshes for each radial functions presented previously. Linear isoparametric boundary elements were used, with double nodes in corners. As an error measure, the relative percentage difference between the value obtained by the DIBEM and the value of the reference solution is calculated for each frequency. The denominator is given by the frequency calculated using the reference solution. The routine for calculating eigenvalues is based on the Heisenberg algorithm for non-symmetric matrices, implemented in FORTRAN language.

5.1 First example – Thinning effect on a membrane

In this first example the performance of the DIBEM is evaluated when the domain presents thinness characteristics. It is well known that the MEC becomes disadvantageous in cases where large boundary extensions limit relatively small portions of the domain. Moreover, its mathematical structure correlates all nodal points of the discretization, i.e., source points interact with distant field points, predisposing to the ill conditioning of the discrete system of equations. Some tests have shown that in problems governed by the Poisson equation (Loeffler and Mansur, 1988) with moderately slender (length about five times the thickness value) the results are still quite satisfactory. However, considering the Helmholtz equation, it is expected that the matrices generated by the DIBEM presents even greater problems, but whose magnitude can only be evaluated after the experimental investigation.

Initially, a rectangular domain of unit sides is considered, in which only prescribed Dirichlet conditions are prescribed with value equal to zero, as shown in figure 1 below:

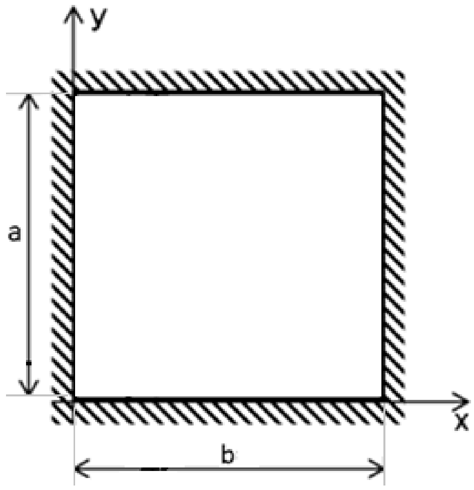

Figure 1. Membrane completely clamped at its boundaries

In this case, the degrees of freedom required for dynamic analysis are given by the internally allocated source points, which also correspond to the basis of radial functions. The stiffness k was considered unitary, as well as the value of dimension a. The value of b is considered in three different values: b = a; b = a/2 and b = a/4.

In the first set of test, the dimensions of the 320 linear boundary elements, that have equal size in the square membrane, are purposefully reduced on the vertical lines, as well as the spacing between the 720 basis points. Figure 2 shows the meshes in these three cases.

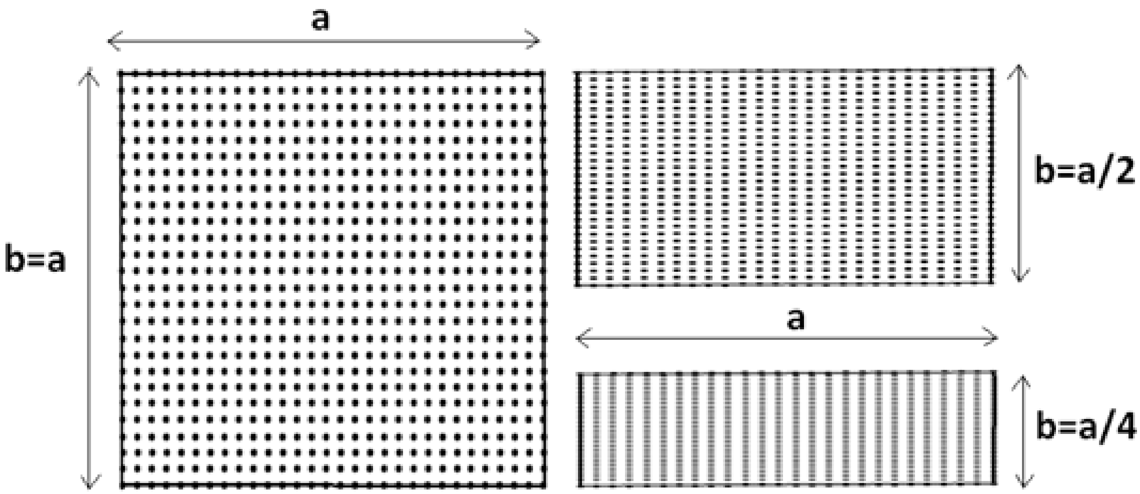

Figure 2. Meshes with 320 boundary elements and 720 basis points in three different geometric configurations

The first twenty eigenvalues were calculated by the DIBEM for each situation and their values were compared with the analytical values, which are determined by the following formula:

$$\omega_{mn} = \pi\sqrt{\frac{m^2}{a^2} + \frac{n^2}{b^2}} \tag{15}$$

The eigenvalues correspond to the natural frequencies of the completely fixed membrane. They are given by the different values of m and n (m, n = 1, 2, 3, ...) and each of these can be associated with vibrational modes.

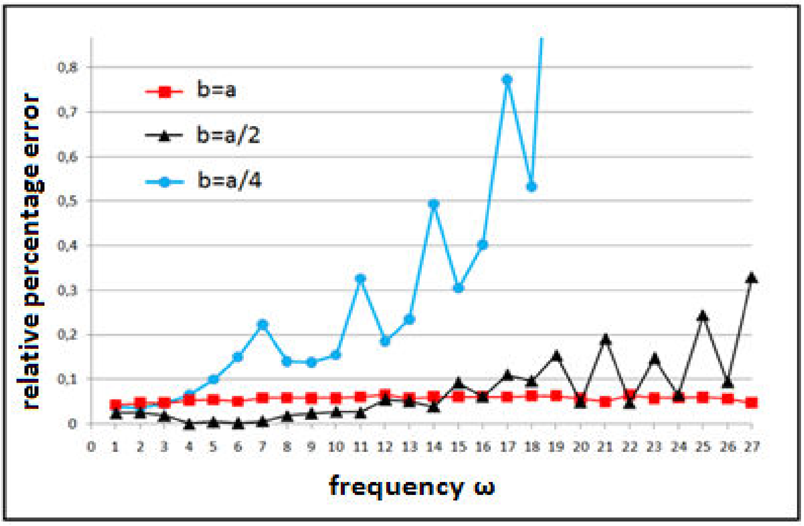

Figure 3. Relative percentage error curves for natural frequencies for three different values of b/a

Initially, the results using the thin-plate interpolation function are presented for the three different meshes. The graph shown in Figure 3 shows the relative error curves.

It can be seen that for the ratio b = a / 4 the errors are much larger than for the other ratios, exceeding 1% in error in the nineteenth frequency. Interestingly, the ratio b = a / 2 shows the smallest percentage errors up to the fourteenth frequency; from this, the results for b = a are always better and it can be seen that they remain practically at the same magnitude during the whole interval examined here. As expected, the results worsened with increasing domain slenderness but the boundary elements on the vertical edges have simply been reduced without any transition, which is inadequate. Moreover, the positioning of the basis points on the inside interferes with the representation of the inertia, that is, the density of these in one region over another reduces the quality of the results. Thus, new tests should be implemented using different strategies.

Considering the same amount of boundary elements and interpolating internal points, the case where b = a / 4 is solved again, but in two different ways: (i) using boundary elements with the same size, but keeping the layout of points inside previously used; (ii) using boundary elements with the same size, but with the arrangement of the internal basis points is distributed evenly in the domain. These results are compared with the heterogeneous mesh used in the previous simulation (iii). For clarity, the arrangement (ii) is shown in Fig.4.

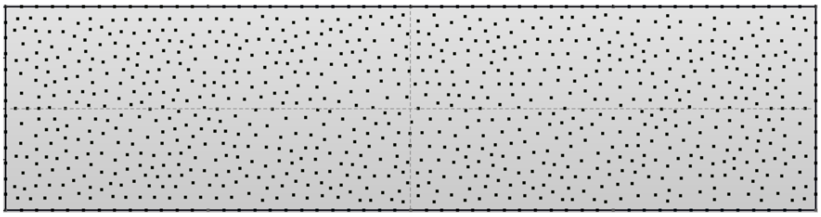

Figure 4. Mesh with 320 boundary elements with same size and 720 basis points distributed evenly

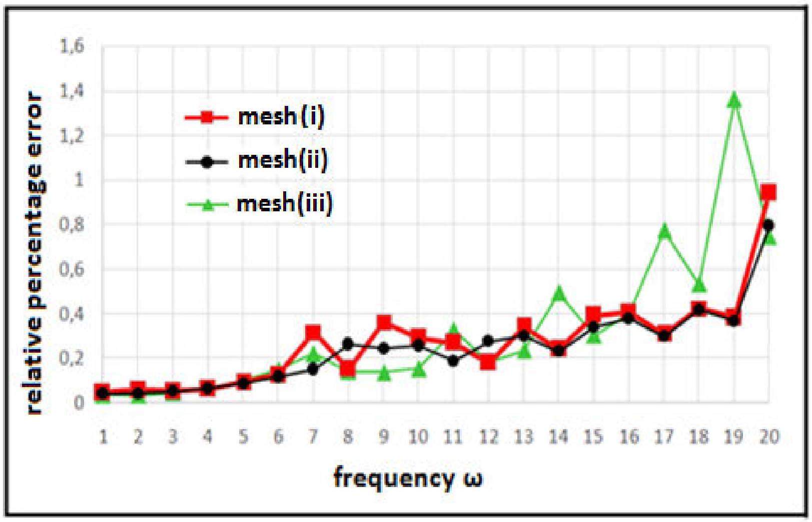

Figure 5. Relative percentage error curves for natural frequencies for three different arrangement of basis points considering b=a/4 using the thin plate radial basis function

The graph of Fig. 5 shows the results of the relative percentage error for these new simulations. A reasonable improvement in performance is observed for the two meshes that have boundary elements with same size - curves (i) and (ii) - especially for the higher frequencies. Just a very slightly improvement have been observed by the uniform distribution of the internal basis points given by the mesh (ii).

The performance of Wendland function was inferior that of the thin plate function, as shown in the graph of Fig. 6. Just the relative error curves for the square membrane and the membrane with b = a / 4 are presented. For this latter, regular boundary meshes and the more It can be seen that numerical errors grow a lot for high frequencies uniform distribution of internal points were considered (case (ii) above).

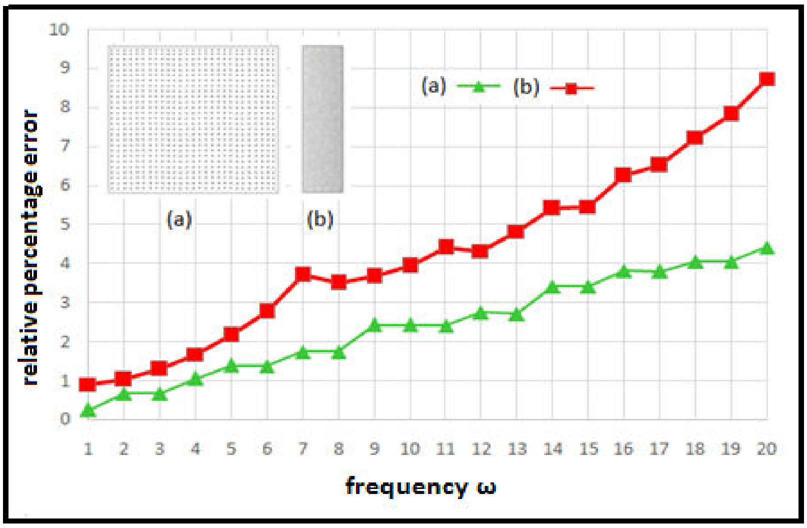

Figure 6. Relative percentage error curves for natural frequencies for three different arrangement of basis points considering b=a/4 using the Wendland radial basis function

5.2 Second example: effect of a groove in a trapezoidal domain

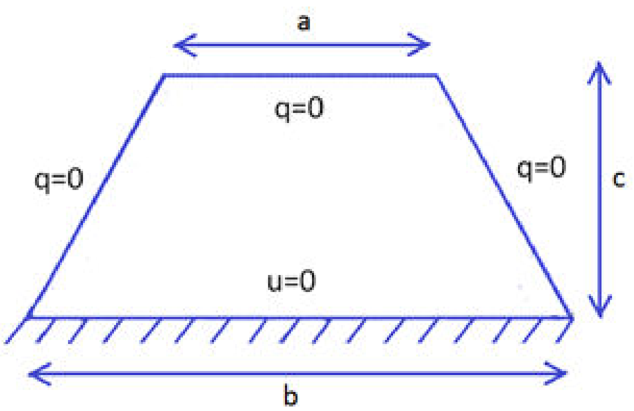

Figure 7. Geometrical features and boundary conditions imposed on the trapezoidal domain without slot.

The purpose of this second example is to quantify the effect of a groove in the numerical results obtained by the DIBEM formulation. Thus, initially a trapezoidal domain without slot is solved, in which the potential in its base is prescribed with null value, while in the other parts of the boundary normal null derivativesare imposed, as shown in Fig. 7. The dimensions considered were a = 1, b = 2 and c = 0.9 units in length.

Three boundary element meshes were used to simulate this problem: the first with 164 boundary nodal points (BN) and 345 internal basis points (IBP); the second with the same 164 nodal points on the boundary, but with 697 basis points; and the third with 364 boundary nodal points and 910 internal basis points. Double nodes are used in all the corners. In the absence of ananalytical solution, the results are compared with solution obtained with the BEM, using a finer mesh with 12228 linear elements and 6305 nodal points.

For a better visualization of the discretizations adopted, the FEM mesh and the finer boundary element mesh are shown in Fig.8.

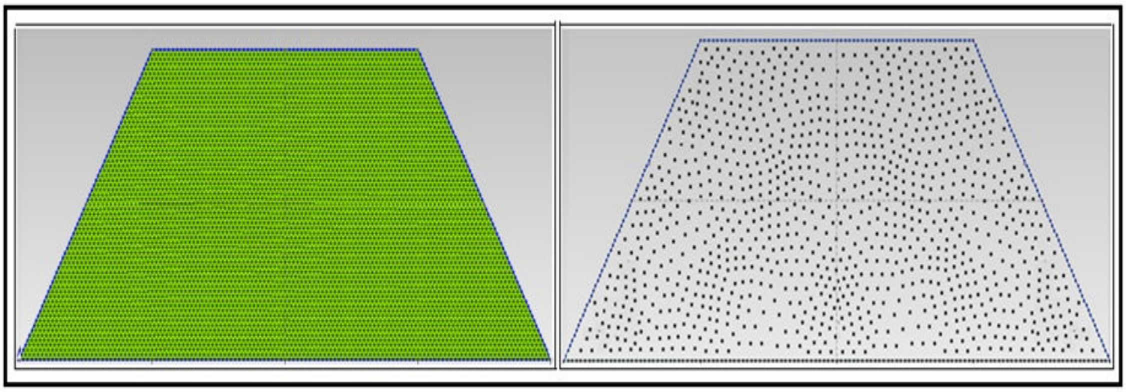

Figure 8. On the left hand side, the FEM mesh; on the right hand side, the finer BEM mesh

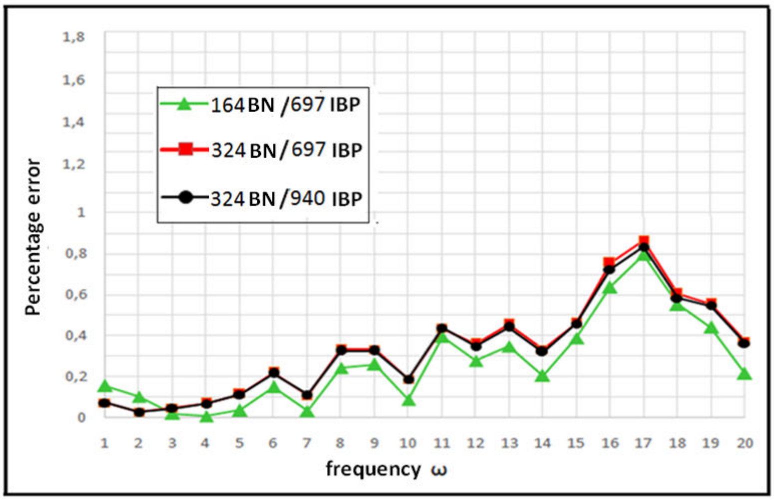

Figure 9. Relative percentage error of the DIBEM results relatively to the FEM results, using the thin plate radial basis function BN

The DIBEM results using thin plate radial function are shown in Fig. 9. It is observed that the relative errors obtained for all BEM meshes presented good precision relatively to the reference solution given by the FEM. Surprisingly, the simpler mesh produced better results, within the considered range of calculated frequencies. It is possible that such behavior is related to the excessive amount of interpolating points on the boundaryagainst the density of the basis points located inside.

Using the Wendland radial basis function, a sensible rising in the errors can be noted comparatively to the error achieved with thin-plate function, as can be seen in Fig. 10.

The best performance also corresponded to the less refined contour mesh, with fewer interpolating internal points.

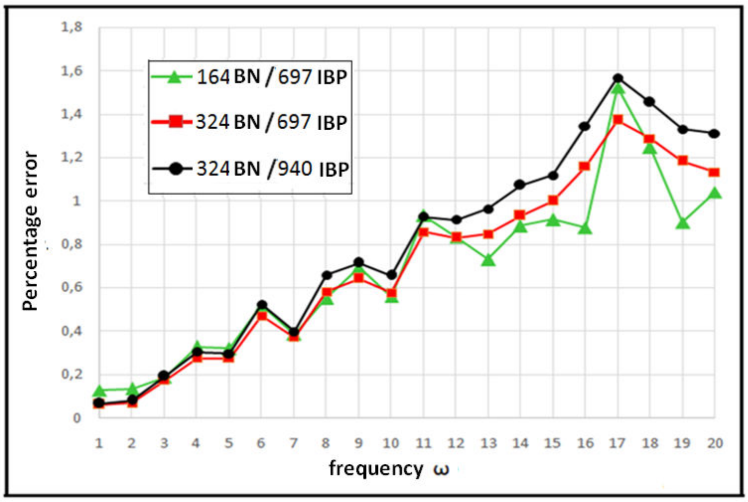

Figure 10. Relative percentage error of the DIBEM results relatively to the FEM results, using the Wendland radial basis function

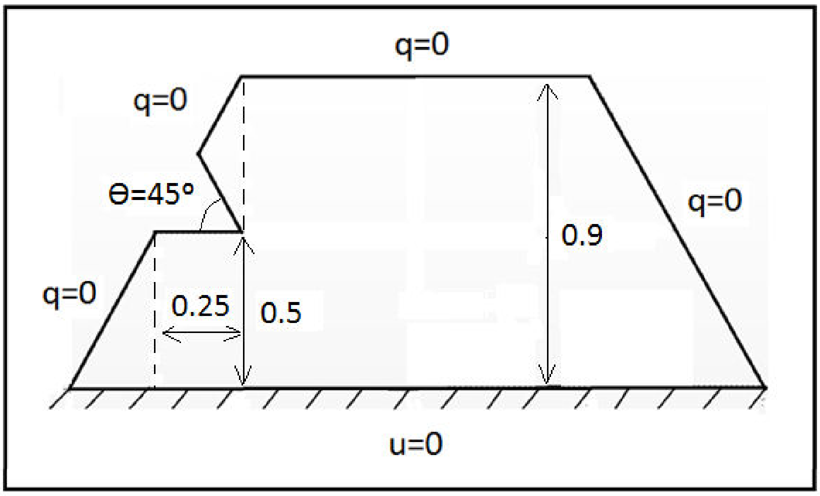

Figure 11. Geometrical features and boundary conditions of the trapezoidal domain with a groove on the left edge.

The following simulations address the same trapezoidal domain in which a groove was introduced at the right edge, as shown in Fig. 11. The dimensions of the upper and lower base were maintained, as well as the applied boundary conditions.

The mesh of the MEF used for comparison has 5293 nodal points and 10292 triangular elements, while the three BEM meshes have 183 and 343 boundary nodes, with 703 or 983 basis points in the interior. Double nodes are used in all the corners. The most refined BEM mesh is shown toghether the FEM mesh in Fig. 12 for clarity.

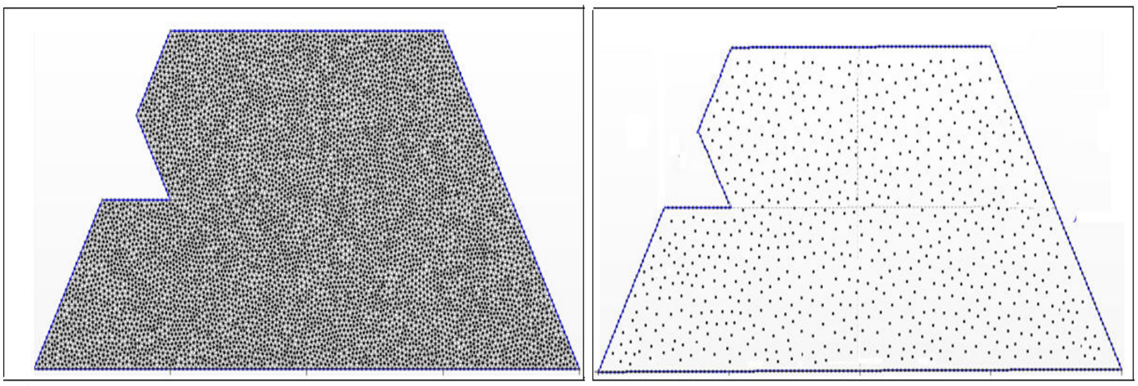

Figure 12. On the left hand side, the FEM mesh; on the right hand side, the finer BEM mesh

Differently from the previous example, the MEC mesh with fewer boundary elements had not good performance, as can be observed in Fig. 13, in which the thin-plate function was used. This indicates that the presence of the groove indeed produces effects that require a greater refinement on the boundary in order to achieve adequate accuracy. Results for the mesh with 343 boundary nodes were very superior but the number of internal basis points did not affect the performance within the range of calculated frequencies.

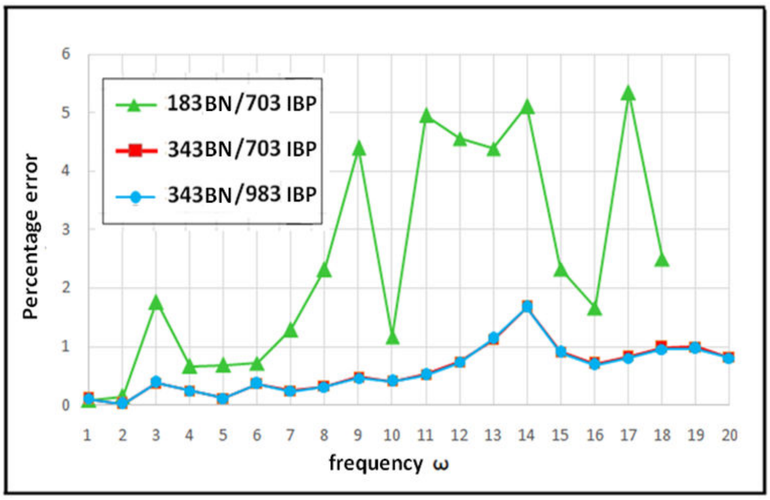

Figure 13. Relative percentage error of the DIBEM results relatively to the FEM results, using the thin plate radial basis function for solving the trapeze with groove.

The simulation using the fully supported Wendland radial basis function repeated the performance of the previous example showing larger errors than the thin plate radial basis function, especially for the range beyond the fourteenth frequency, as shown in Fig. 14. Just the results for the finer boundary mesh are presented.

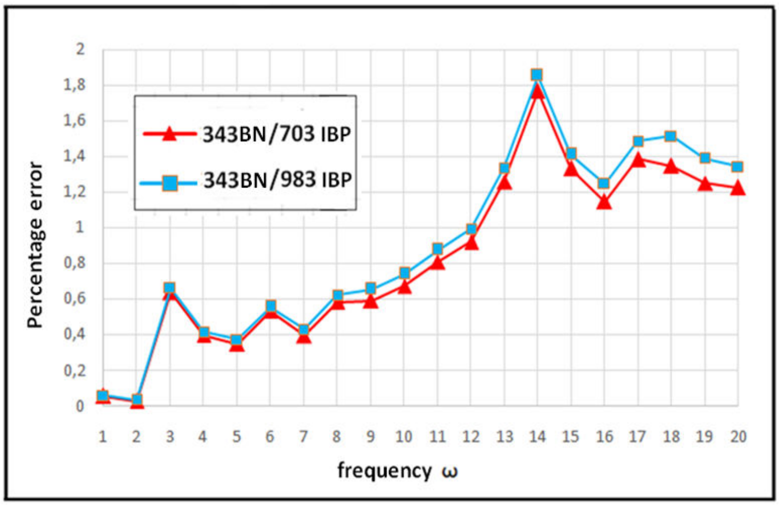

Figure 14. Relative percentage error of the DIBEM results relatively to the FEM results, using the Wendland radial basis function for solving the trapeze with groove.

Comparatively to the previous example, the DIBEM errors have increase due to the insertion of the groove, as expected. Despite the meshes used now and latter to be different, the number of boundary elements and internal basis points is very similar.

5.3 Third example: domain with X shape

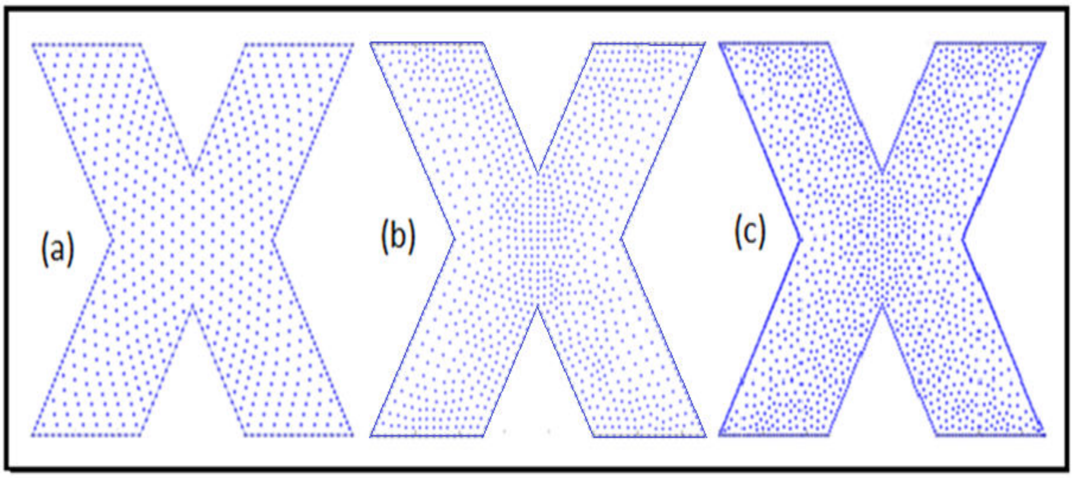

Figure 15. Three boundary element meshes used for solving the third example.

In this example theability of the DIBEM to to solve problems with several corners is evaluated. Thus, a domain in the form of X was solved by using three different meshes with linear elements and double nodes in all the corners, as shown in Fig. 15:

The mesh (a) has 268 nodal points and 529 internal interpolating points; the mesh (b) has the same 268 nodal points with a greater number of interpolating points: 817; in the third mesh (c) both the number of nodal points and the number of interpolating points was increased, with 524 nodes located on the boundary and 1043 interpolation points placed in the interior. To generate numerical results for comparison with the DIBEM, a MEF mesh with 2283 nodes and 4308 triangular elements with linear interpolation was used, as shown in Fig. 16.

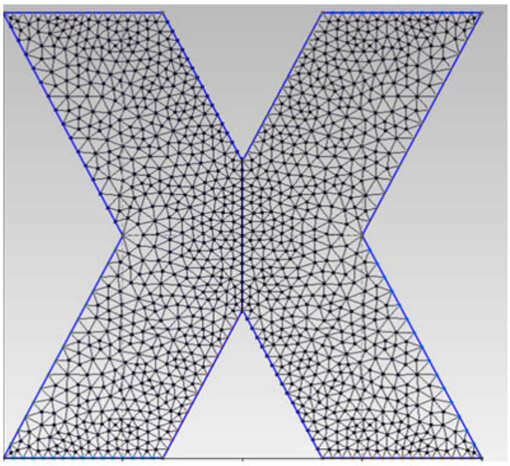

Figure 16. Finite Element mesh used to provide a reference solution for the third example

For the DIBEM, the two radial basis functions previously presented were used. The results for the thin-plate function are shown in Fig. 17 whilst the results for the Wendland Function are shown in Fig. 18.

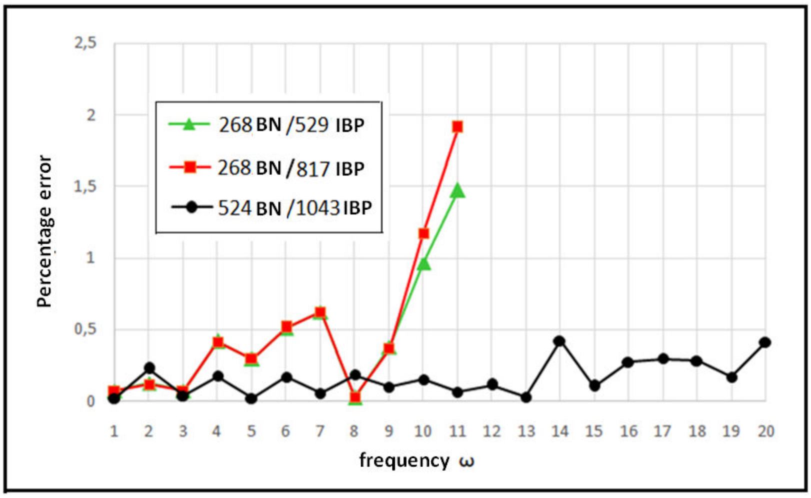

Figure 17. Percentage error of the DIBEM using thin plate radial basis function relatively to the FEM solution for the X problem

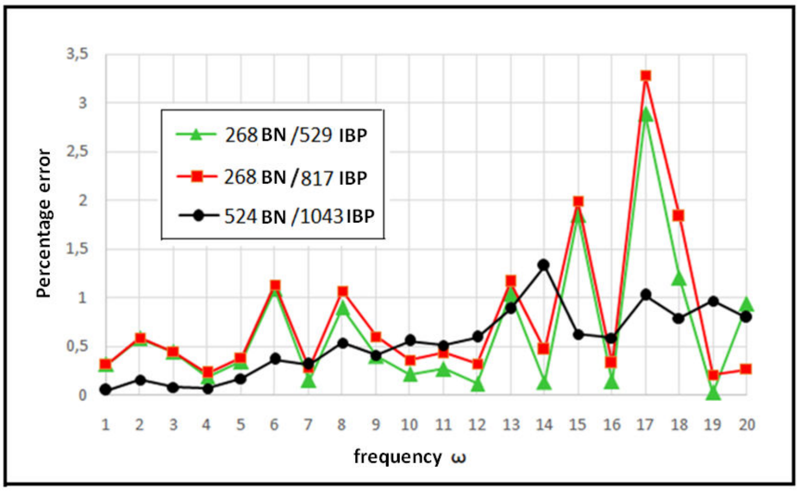

Figure 18. Percentage error of the DIBEM using Wendland radial basis function relatively to the FEM solution for the X problem

In this case where the boundary shape is more intricate the performance of the Wendland function was markedly higher in simulations using poorer meshes. Only in the simulation with the most refined mesh was used the thin plate function has presented good results, which were the best in the computation of all the simulations performed. One can not exactly identify the reason why Wendland function responds relatively better than the thin plate function in this case; however, it is suspected that considering the less elaborate discretizations, the better conditioning of the matrix system provided by Wendland function is the most relevant factor.

6 CONCLUSIONS

Initially, it should be emphasized that in the case of dynamic problems, a high amount of degrees of freedom is required in order to obtain a frequency spectrum with relative precision. This is evidenced in the case of DIBEM, where a high number of internal points is required especially for good interpolation of the inertia property. However, the results shown showed good similarity to the values obtained with MEF, in which meshes with a much greater number of degrees of freedom were used.

With respect to the radial functions tested, it can be verified that the model generated by the Wendland function produced results inferior to those obtained by the thin plate function, except for the last example, in which the boundary had multiple corners. In this, probably because the function of Wendland generate interpolation matrices with the dominant diagonal, a more precise solution of the non-symmetric matrix system of the MEC was obtained in the conditions of coarse refinement.

The slenderness effect evaluation tests indicated that the uniformity in the size of the boundary elements has a more pronounced effect than the regular distribution of the basis points in the interior, although the better disposition of these will also contribute to improved results. In these simulations, the thinplate radial basis function performed well above the Wendland function.

The effect of the boundary cutout also influenced the DIBEM results in the case of trapezoidal geometry. Although the percentage errors grew only slightly for the most refined meshes, the poorest boundary meshes no longer had the same good performance presented in the simulation of the trapezium without notching.

In summary, the results of the DIBEM were also quite satisfactory in the solution of these problems in that the geometric conformation is not so simple within the frequency spectrum presented. Although not presented, the results show increasing error, as in any numerical method, but without instabilities of any order. The determination of spurious - negative or complex - frequencies occurs in a higher range of eigenvalues, as a result of numerical inaccuracies of a method that deals with non - symmetric matrices.

It is noteworthy that DIBEM, despite requiring a greater number of internal points than similar formulations such as Dual Reciprocity, shows no instability with the refinement of the mesh and insertion of internal basis points. In some cases, the simpler meshes may present better results due to both the more favorable positioning of the internal points and the better arrangement of them in relation to the boundary nodes, which also act as interpolating points.

REFERENCES

Braga, C., L., R., 2006. Physical-Mathematics Notes (in portuguese). Editora Livraria da Física, São Paulo.

Brebbia, C., A., & Dominguez, J., 1992. Boundary Elements: An Introductory Course, WIT Press. Southampton.

Brebbia, C., A., & Walker, S., 1980. Boundary Element Techniques in Engineering.Newnes-Butterworths, London.

Buhmann, M., D.,2003. Radial Basis Function: Theory and Implementations, Cambridge Press, Cambridge..

Chen, C., S., Brebbia, C., A., & Power H., 1999. Dual Reciprocity Method Using Compactly Supported Radial Basis Functions. Commun.Numer.Meth.Engng, v. 15, pp.137-150.

Loeffler, C., F., Zamprogno, L., Mansur, W., J., & Bulcão, A., 2016. Performance of Compact Radial Basis Functions in the Direct Interpolation Boundary Element Method for Solving Potential Problems.Approved for publishing in Computational Methods and Engineering and Sciences.

Loeffler, C., F., Mansur, W., J., Barcelos, H.,M., & Bulcão, 2015. Solving Helmhotz problems with the boundary element method using direct radial basis function interpolation. Engineering Analysis with Boundary Element, v.61,pp. 218-225.

Loeffler, C., F., Cruz, A., L., &Bulcão, A., 2015. A. Direct Use of Radial Basis Interpolation Functions for Modelling Source Terms with the Boundary Element Method. Engineering Analysis with Boundary Elements, v. 50, pp. 97-108.

Loeffler, C., F., &Mansur, W., J., 1987.Analysis of Time Integration Schemes for Boundary Element Applications to Transient Wave Propagation Problems. In: C.A. Brebbia (Ed.), Boundary Element Techniques: Applications in Stress Analysis and Heat Transfer, Computational Mechanics Publishing, UK, pp. 105-124.

Nardini, D., & Brebbia, C., A., 1983. Transient Dynamic Analysis by the Boundary Element Method, in C.A. Brebbiaed, Proceedings of BEM V, pp 719-730.

Partridge, P., W., Brebbia, C., A., & Wrobel, L., C., 1992. The Dual Reciprocity Boundary Element Method. Computational Mechanics Publications and Elsevier, London.

Schaback, R., 2007.A practical guide to Radial Basis Functions. http://num.math.uni-goettingen.de/schaback/teaching/texte/approx/sc.pdf.

Wendland, H., 1995. Piecewise polynomial, positive definite and compactly supported radial functions of minimal degree, *Adv. in Comput. Math*., vol.4, pp. 389-396.

Wu, Z., 1995. Compactly supported positive definite radial functions. Adv. in Comput. Math., v. 4, pp. 283-292.